Density-functional description of water condensation in proximity of nanoscale asperity

Pavel B. Paramonov and Sergei F. Lyuksyutov[a)]
Departments of Physics and Polymer Engineering, The University of Akron, Akron, Ohio 44325

(Received 15 April 2005; accepted 30 June 2005; published online 30 August 2005)

We apply nonlocal density-functional formalism to describe an equilibrium distribution of the waterlike fluid in the asymmetric nanoscale junction presenting an atomic force microscope tip dwelling above an arbitrary surface. The hydrogen bonding dominating in intermolecular attraction is modeled as a square-well potential with two adjustable parameters (energy and length) characterizing well's depth and width. A liquid meniscus formed inside the nanoscale junction is explicitly described for different humidity. Furthermore, we suggest a simple approach using polymolecular adsorption isotherms for the evaluation of an energetic parameter characterizing fluid (water) attraction to substrate. This model can be easily generalized for more complex geometries and effective intermolecular potentials. Our study establishes a framework for the density-functional description of fluid with orientational anisotropy induced by nonuniform external electric field. © *2005 American Institute of Physics*. [DOI: 10.1063/1.2007632]

I. INTRODUCTION

An equilibrium behavior of a fluid near geometrically nonuniform solid surfaces exhibits various peculiarities related to confinement and spatially varying external potentials. A quantitative understanding of water condensation phenomena in proximity of nanoasperities under ambient humidity is important for different areas of research including scanning probe microscopy (SPM), nanopatterning, adhesion, and friction at macro- and nanoscale. Specifically, the formation of liquid films and bridges near an asperity of submicro- or nanoscale curvature has to be adequately described.

An importance of the water condensation phenomenon from ambient atmosphere into nanoscale junction formed by atomic force microscope (AFM) tip dwelling above surface has been recognized in number of works.[1–10] The formation of the water meniscus affects strongly the force-distance measurements and AFM imaging resolution,[1,2] provides nanoscale electrochemical cell for SPM oxidation of semiconductors and metals,[3,4] serves as ink transport channel for dip-pen nanolithography,[5,6] and plays an essential role in AFM-assisted electrostatic nanolithography (AFMEN) on thin polymer films.[7–10]

Direct experimental observations of meniscus formation in the AFM tip-surface junction are complicated due to nanometer-scale size of the region of interest. There are no optical tools available for this purpose due to the wavelength limitation. Indirect estimations of the meniscus's size can be made using SPM oxidation,[3] noncontact AFM imaging,[11,12] and substrate's dissolution in water.[13] Several theoretical estimations of the meniscus size and shape based on either macroscopic Kelvin equation[14,15] or molecular level grand canonical Monte Carlo simulations[16–18] have been performed. A macroscopic phenomenological approach based on the modifications of the Kelvin equation has been suggested to describe water attracted to biased AFM tip.[12] The model misses molecular level understanding, and is not applicable for the systems confined to the several molecular diameters[19,20] typical for AFM tip-substrate separation. Arguably, the approaches based on the Kelvin equation do not account strongly adsorbed layers, and neglect the density oscillations near the confining surfaces.[20]

The goal of this work is to develop a versatile description of the water condensation in proximity of a nanoscale asperity and investigate the influence of spatially nonuniform external electric field, with focus on SPM lithography. In the current study, we concern with the case of isotropic fluid confined in asymmetric nanojunction in the absence of the electric field to develop a basic framework for the case of field-induced orientational anisotropy.

Typical molecular approaches, applicable to the problem of our interest, include Monte Carlo-type[21] and molecular-dynamics-type[22] computer simulations, and also density-functional theory (DFT).[23,24] A grand canonical Monte Carlo simulation of water condensation in the context of the dip-pen nanolithography has been reported by Jang *et al.*[16–18] including clarification of fluctuations in the meniscus width. The influence of relative humidity, AFM tip curvature, tip and substrate wetting properties on the meniscus size, and capillary force have been studied.

Unlike other studies, our work concerns with DFT approach to model real systems in which the fluctuations of meniscus's width, as established in Ref. 16, are not significant. A mean-field character of the DFT is appropriate since the fluid is considered far from the critical point.

Another reason for DFT choice with respect to Monte Carlo technique is the convenience of generalization to the case of the electric-field-induced anisotropy. The Monte Carlo simulations with additional orientational degrees of

[a)]Electronic mail: sfl@physics.uakron.edu

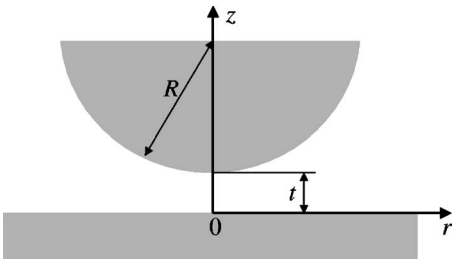

FIG. 1. A schematic presentation of the nanoscale junction consisting of a planar surface and a spherical asperity with curvature of the radius R, separated by the distance t. A fluid is nonuniformly distributed in the junction. The configuration resembles an AFM tip dwelling above the surface.

freedom require special care to avoid local minima and to ensure proper sampling of configurational space. This leads to increased computational time in the case of the low acceptance rates at the regions filled with a dense liquid. Molecular-dynamics approach was not used because of the variable number of particles dictated by the type of the problem. Second reason was such that the low densities in the vapor phase provide insufficient number of collisions for proper statistical averaging. Additionally, the formulation of the analytical expressions, possible in the framework of DFT, is highly desirable. Another advantage of DFT is a consistency in mapping of the three-dimensional (3D) geometry into the quasi-two-dimensional (2D) description. This helps to avoid errors in quantitative prediction of the solvation forces existing in the case of 2D lattice Monte Carlo simulation.[17]

The paper is organized as follows. Section II is the model and methodology. The first part of this section describes the model including nonlocal density-functional formulation and specifics of fluid, while the second part outlines the computational issues related to the form of the integral equation for density distribution. We discuss multidimensional integrals handling, and describe the iterative procedure developed. Section III A concerns with elucidation of the model parameters of the fluid from the bulk behavior. Section III B presents the results of the calculations. The meniscus's size and its variation with respect to the relative humidity and wall separation are discussed. Section III C addresses determination of the fluid-wall interaction parameters to link the model's calculations to particular physical systems. The procedure is based on the polymolecular adsorption isotherms. Section IV presents the summary.

II. MODEL AND METHODOLOGY

A. Model description

The nanoscale junction consists of planar surface and spherical asperity of the radius R, separated from the surface at the distance t (Fig. 1). The choice of the cylindrical coordinate system is related to the azimuthal symmetry of the problem. The fluid is nonuniformly distributed in the junction.

The purpose of the equilibrium DFT applied to the inhomogeneous fluid is to find the spatial distribution for the number density of molecules $\rho(\mathbf{r})$ by minimizing the grand potential Ω, presented as a functional of $\rho(\mathbf{r})$ for the grand canonical (T,V,μ) ensemble,[23,24]

$$\Omega[\rho(\mathbf{r})] = F[\rho(\mathbf{r})] + \int \rho(\mathbf{r})(V_{\text{ext}}(\mathbf{r}) - \mu)d\mathbf{r}. \tag{1}$$

An intrinsic Helmholtz free-energy functional $F[\rho(\mathbf{r})]$ incorporates the properties of fluid. In general case, the functional depends on the external potential $V_{\text{ext}}(\mathbf{r})$ if the intermolecular forces and/or intramolecular degrees of freedom are affected by the external field. However, we defer this discussion to the second part of the study, and consider $F[\rho(\mathbf{r})]$ invariant with respect to $V_{\text{ext}}(\mathbf{r})$. The external potential describes the solid surfaces in contact with fluid thus inducing inhomogeneity in the system. The chemical potential μ is related to the ambient humidity.

The Helmholtz free-energy functional $F[\rho(\mathbf{r})]$ can be presented as

$$F[\rho(\mathbf{r})] = F_{\text{id}}[\rho(\mathbf{r})] + \Delta F_{\text{rep}}[\rho(\mathbf{r})] + \Delta F_{\text{attr}}[\rho(\mathbf{r})], \tag{2}$$

where $F_{\text{id}}[\rho(\mathbf{r})]$ corresponds to the ideal system without intermolecular interactions, and the other two terms describe the additional intermolecular repulsion and attraction, respectively. The ideal part of the Helmholtz free-energy functional is given explicitly by

$$F_{\text{id}}[\rho(\mathbf{r})] = kT \int \rho(\mathbf{r})\left(\ln(\lambda_{\text{th}}^3\rho(\mathbf{r})) - 1 + \frac{\mu_{\text{int}}}{kT}\right)d\mathbf{r}, \tag{3}$$

where λ_{th} is a thermal wavelength, k is the Boltzmann constant, and T is the temperature. The term $\mu_{\text{int}}(kT)^{-1}$ has been added to incorporate the internal degrees of freedom of the water molecules.

The repulsive free-energy functional is expressed as

$$\Delta F_{\text{rep}}[\rho(\mathbf{r})] = \int \rho(\mathbf{r})\Delta\psi_{\text{hs}}(\bar{\rho}(\mathbf{r}))d\mathbf{r}. \tag{4}$$

Here $\Delta\psi_{\text{hs}}$ is an excess free-energy density for the repulsive fluid evaluated at every spatial point as a function of smoothed (coarse-grained) density $(\bar{\rho}(\mathbf{r}))$. The latter is an average of the local density $\rho(\mathbf{r})$ taken over a small domain using the weighting function ω,

$$\bar{\rho}(\mathbf{r}) = \int \rho(\mathbf{r}')\omega(|\mathbf{r} - \mathbf{r}'|,\ldots)d\mathbf{r}'. \tag{5}$$

The weighting function depends on ρ according to the particular nonlocal DFT formulation.[23] We use the repulsive intermolecular potential with a hard-sphere diameter σ and the Carnahan-Starling free-energy density[25]

$$\Delta\psi_{\text{hs}} = kT\frac{4\eta - 3\eta^2}{(1-\eta)^2}, \tag{6}$$

where η is the packing fraction of the hard spheres corresponding to the number density ρ,

$$\eta = \frac{\pi}{6}\sigma^3\rho(\mathbf{r}). \tag{7}$$

For the sake of simplicity we choose a generalized van der Waals model[23,26] with

$$\omega(|\mathbf{r}-\mathbf{r}'|) = \frac{3}{4\pi\sigma^3}\theta(\sigma-|\mathbf{r}-\mathbf{r}'|), \tag{8}$$

where θ is a Heaviside step function. While some other approaches, such as the Tarazona's model,[27] have better accuracy for describing density profiles of the hard-sphere systems, the choice of the generalized van der Waals model is justified in the systems with strong intermolecular attraction,[26] which is the case of our interest.

In the framework of the mean-field approximation, the third term in Eq. (2) describing an attractive part of the free-energy functional can be written as

$$\Delta F_{\mathrm{attr}}[\rho(\mathbf{r})] = \frac{1}{2}\iint \rho(\mathbf{r})\rho(\mathbf{r}')\Phi_{\mathrm{attr}}(|\mathbf{r}-\mathbf{r}'|)d\mathbf{r}d\mathbf{r}', \tag{9}$$

where $\Phi_{\mathrm{attr}}(\mathbf{r})$ is the attractive pair intermolecular potential. We consider the waterlike fluid for which $\Phi_{\mathrm{attr}}(\mathbf{r})$ is a square-well potential characterized by two *effective* parameters such as the depth (ϵ), and the width (d) of the well. This choice is related to the fact that in water, the short-range hydrogen bonding dominates the longer-range dipole-dipole and higher-order interactions. Similar forms of attractive potentials were used before.[28,29] The main advantage of the square-well attractive potential is its relative simplicity for the DFT calculations. At the same time, it effectively conveys the major contribution to the intermolecular attraction in water, as indicated, for example, by reasonable predictions of the second virial coefficient.[29]

The minimization of the functional given by Eq. (1) with $F[\rho(\mathbf{r})]$ presented above by Eqs. (2)–(9) leads to the following integral equation for the equilibrium density profile $\rho(\mathbf{r})$:

$$kT(\ln(\lambda_{\mathrm{th}}^3\rho(\mathbf{r})) - 1) + \mu_{\mathrm{int}} + \Delta\psi_{\mathrm{hs}}(\bar{\rho}(\mathbf{r})) + J_{\mathrm{hs}}[\rho(\mathbf{r}),\bar{\rho}(\mathbf{r})] + J_{\mathrm{int}}[\rho(\mathbf{r})] + V_{\mathrm{ext}}(\mathbf{r}) = \mu, \tag{10a}$$

$$J_{\mathrm{hs}}[\rho(\mathbf{r}),\bar{\rho}(\mathbf{r})] = \frac{3}{4\pi\sigma^3}\int \Delta\psi'_{\mathrm{hs}}(\bar{\rho}(\mathbf{r}'))\,\theta(\sigma-|\mathbf{r}-\mathbf{r}'|)\rho(\mathbf{r}')d\mathbf{r}', \tag{10b}$$

$$J_{\mathrm{int}}[\rho(\mathbf{r})] = -\epsilon\int \theta(|\mathbf{r}-\mathbf{r}'|-\sigma)\,\theta(d-|\mathbf{r}-\mathbf{r}'|)\rho(\mathbf{r}')d\mathbf{r}', \tag{10c}$$

where $\Delta\psi'_{\mathrm{hs}}$ in (10b) denotes the differentiation with respect to ρ. Equation (10a) is to be solved for $0\leqslant r\leqslant L$, $0\leqslant z\leqslant t+R-\sqrt{R^2-r^2}$, and $0\leqslant\phi\leqslant 2\pi$. The boundary $r=L$ is chosen such that the region within which the liquid bridge may be formed corresponds to $r\ll L$.

An explicit form of the external potential $V_{\mathrm{ext}}(\mathbf{r})$ describing interaction of the fluid with the confining surfaces is the final piece required for closure of the model's description. For that we use a two-parametric exponential attraction potential on top of the hard-wall repulsion,

$$V_{\mathrm{ext}}(x) = \begin{cases} -\epsilon_s\exp(-\alpha x), & x\geqslant 0, \\ \infty, & x<0, \end{cases} \tag{11}$$

where x is the distance from the surface. Both planar wall and spherical asperity interact with the fluid according to (11); in the latter case, x is the distance along the normal to the spherical surface. The parameter ϵ_s is the work required to displace a water molecule from $x=0$ to infinity corresponding to the binding energy of water at a given surface. The selected form (11) of the fluid-wall potential is convenient for calculations, and is capable of describing partial/complete wetting transition as ϵ_s is varied.[30] The detailed form of V_{ext} in the spatial region $0<x\leqslant\sigma$ does not have a significant effect on the results for liquid meniscus condensation as long as the binding energy ϵ_s is kept constant.

B. Computational part

The triple integrals (10b) and (10c) must be evaluated over the 3D volume. Fortunately, the character of their angular dependence in a step-function form reduces them to the double integrals below:

$$\iiint u(\mathbf{r})\,\theta(p-|\mathbf{r}-\mathbf{r_0}|)d\mathbf{r} = \int rdr\int dz\cdot 2\lambda u(r,z), \tag{12a}$$

$$\lambda = \begin{cases} \arccos(\Lambda), & -1<\Lambda<1, \\ 0, & \Lambda\geqslant 1, \\ \pi, & \Lambda\leqslant -1, \end{cases} \tag{12b}$$

$$\Lambda = \frac{(z-z_0)^2+r^2+r_0^2-p^2}{2rr_0}. \tag{12c}$$

The iterative method used to solve the nonlinear integral in Eq. (10a) deserves special description. Simple successive approximation procedure normally fails for the equations similar to (10a) even for one-dimensional problems as the computation diverges after the few iterations.[26,27] Several approaches were used to overcome this difficulty for the one-dimensional case. Tarazona[27] used the mixing of the new and previous iterative values with a space-dependent mixing function. While this approach fixes divergence, it requires a careful selection of the mixing function through trial end error, and converges slowly. Vanderlick *et al.*[26] used a uniform discretization of the domain and converted an integral equation into the system of nonlinear algebraic equations. This approach works well for one-dimensional problems, but depends on the choice of the discretization method.

In our model, the spatial domain for which Eq. (10a) has to be solved is two dimensional and asymmetric. Below we suggest an iterative scheme conceptually similar to Newton's iterative method for the systems of algebraic equations. The general form of Eq. (10a) can be written as

$$\ln\rho + \Phi(\rho) = B, \tag{13}$$

where $\Phi(\rho)$ has a complicated dependence with respect to ρ. The iterative scheme is set up in the form

$$\ln \rho^{(m+1)} + \Phi(\rho^{(m)}) + (\rho^{(m+1)} - \rho^{(m)})\left(\frac{\partial \Phi}{\partial \rho}\right)_{\rho^{(m)}} = B. \quad (14)$$

Here $\rho^{(k)}$ is an approximation for $\rho(r,z)$ obtained at kth iteration. The integral terms appearing in Φ and its derivative are calculated simultaneously. The equation which has to be solved at mth iteration has the following form:

$$\ln \rho^{(m+1)} + D\rho^{(m+1)} = C, \quad (15)$$

and its solution can be presented via the Lambert W-function:

$$\rho^{(m+1)} = \exp(C - W(De^{C})). \quad (16)$$

We found that the iterative procedure given by Eqs. (14)–(16) is very efficient so that the convergence is often accomplished in less than 10–20 iterations.

III. RESULTS AND DISCUSSION

A. Bulk fluid and model parameters

For the case of the uniform bulk fluid, Eq. (10a) can be reduced to the following form:

$$\mu = kT(\ln(\lambda_{\text{th}}^3\rho) - 1) + \mu_{\text{int}} + \Delta\psi_{\text{hs}} + \rho\Delta\psi'_{\text{hs}} - \frac{4\pi}{3}\left(\left(\frac{d}{\sigma}\right)^3 - 1\right)\rho\sigma^3\epsilon. \quad (17)$$

To determine the parameters σ, d, and ϵ in Eq. (17) we use the characteristics of water at the critical point determined by the following thermodynamic conditions:[31]

$$\left(\frac{\partial \mu}{\partial \rho}\right)_{T_c} = 0, \quad \left(\frac{\partial^2 \mu}{\partial \rho^2}\right)_{T_c} = 0. \quad (18)$$

The derivatives are evaluated at the critical temperature T_c (647 K for water). The solution of these equations with μ explicitly given by Eq. (17) determines two groups of the parameters:

$$\sigma^3\rho_c = 0.2372, \quad \frac{4\pi}{3}\left(\left(\frac{d}{\sigma}\right)^3 - 1\right)\frac{\epsilon}{kT_c} = 10.3882. \quad (19)$$

The density of water under critical point conditions ρ_c results in $\sigma = 2.8$ Å, which is commonly taken as a hard-sphere diameter of water molecule.[29] The separation of the parameters ϵ and d in the second group is not required as they are always grouped together.

The second consideration for the bulk fluid deals with liquid-vapor coexistence at the temperature $T = 300$ K. Two coexistence equations are derived assuming the chemical potential and pressure to be equal for both phases. The chemical potential is given by Eq. (17), and the pressure is presented as a function of number density $P(\rho)$ using the expression for the grand canonical potential Ω for the bulk fluid,

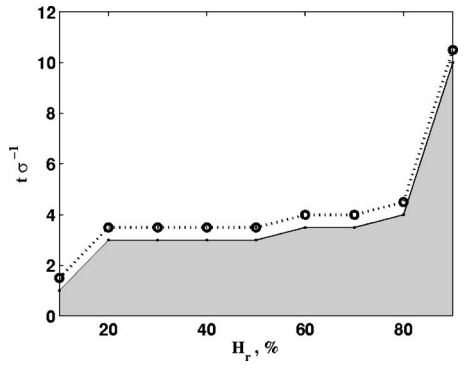

FIG. 2. The condensation of waterlike fluid in between a planar surface and a spherical asperity of the radius $R = 36\sigma$ (10 nm). A shaded area corresponds to the formation of liquid meniscus. The separation distance t varies between σ and 12σ, where $\sigma = 2.8$ Å. No liquid bridge is formed for given H_r when t reaches ordinate of the open circle. The energy of H-bonding ϵ was about 5 kcal/mol. The energy required to remove a single fluid molecule from an adsorbed state was selected $\epsilon_s = \epsilon$. The parameter α was $2/\sigma$.

$$-\frac{\sigma^3}{kT}P = \sigma^3\rho\left(Q + \ln(\sigma^3\rho) + \frac{\Delta\psi_{\text{hs}}}{kT}\right) - \frac{2\pi}{3}\left(\left(\frac{d}{\sigma}\right)^3 - 1\right)\frac{\epsilon}{kT}(\sigma^3\rho)^2, \quad (20)$$

where dimensionless parameter Q was introduced as

$$Q = 3\ln\left(\frac{\lambda_{\text{th}}}{\sigma}\right) - 1 + \frac{\mu_{\text{int}}}{kT}. \quad (21)$$

After solving the equations above, we find $\sigma^3\rho_v = 1.86 \times 10^{-4}$ and $Q = 5.6$ selecting the density of water in the liquid phase at 300 K, $\rho_l = 0.731\sigma^{-3}$. The vapor phase density ρ_v is used as a reference value to calculate chemical potential μ for given relative humidity H_r.

B. Liquid meniscus condensation in the nanoscale junction

The fluid density distribution was calculated, using the methodology above, for the geometry presented in Fig. 1, at different values of relative humidity H_r and separation between confining walls t at $T = 300$ K. It was found that for certain values of H_r and t, the fluid tends condensing in the region near $r = 0$, forming a liquid meniscus connecting the confining surfaces. The tendency for liquid meniscus condensation increases with H_r and decreases with the growth of t. The region in $H_r - t$ coordinates, corresponding to the meniscus formation, is depicted in Fig. 2.

Figure 3 presents the typical fluid density profiles: $\sigma^3\rho$ as a function of the axial coordinate $z\sigma^{-1}$, for different radial positions r. The density profile for given r is determined by the separation between the walls at that point, providing that the fluid-wall interaction parameters are fixed. The fluid density is higher near the walls with several maxima in between (Fig. 3). A significant density redistribution occurs near the meniscus boundary. For the longer radial distances, the liquid wets confining surfaces for specific values of ϵ_s and α.

An important question is how to define the size of the liquid meniscus based on the computed fluid density distribution, or what factors define liquid/vapor boundary for a

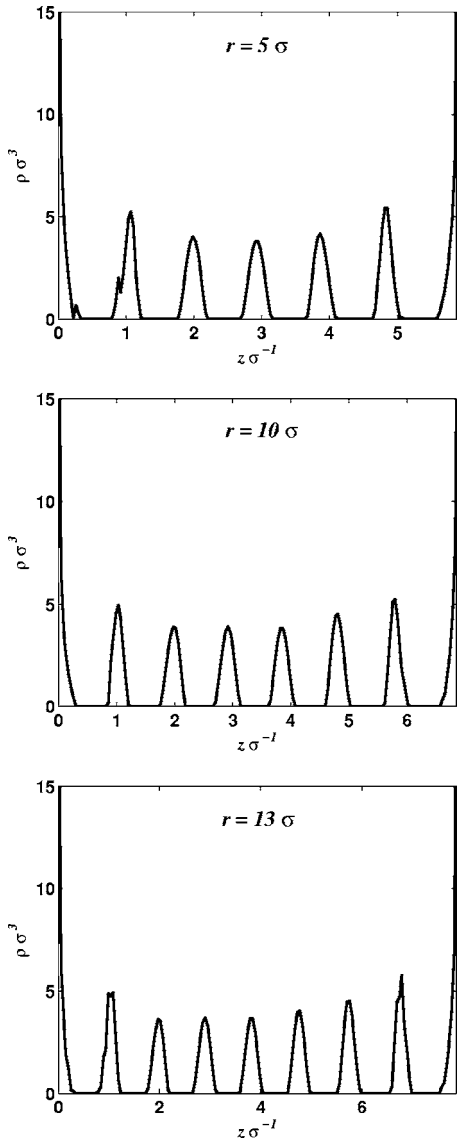

FIG. 3. The profiles of waterlike fluid density between a planar surface and a spherical asperity of the radius $R=36\sigma$ (10 nm), separated at the distance $t=5.5\sigma$, for three different values of the radial coordinate r. A relative humidity was 90%, and the parameters of fluid interaction with solid walls were $\epsilon_s\epsilon^{-1}=1$ and $\alpha\sigma=2$.

smooth density distribution in the asymmetric geometry. The answer can be found should we specify the phenomena of interest and its description based on the dimensions of the liquid bridge. The description of the charge transport in the nanoscale junction and the calculation of the forces exerted by fluid on the confining walls require different effective meniscus radii. A certain approximation is required because this work describes general peculiarities of meniscus formation under variable conditions. In earlier work related to water meniscus formation,[16] an *ad hoc* threshold of half filled lattice site has been used. In our work, we use a single threshold value of the number density to separate liquid and vapor regions, and define the boundary. We assume that if the interaction energy of a fluid molecule located at a given point of space with its neighbors is equal or less than kT, then it belongs to vapor phase, otherwise, to liquid phase. Such an energetic criterion is chosen because the inhomogeneous fluid system of our interest does not exhibit any continuous regions of bulk liquid density ρ_l, and the concept of the liquid-vapor interface cannot be strictly defined, thus excluding the possibility of using traditional thermodynamic definitions of the liquid/vapor dividing surfaces. The corresponding quantitative criterion can be presented using Eq. (10c) as

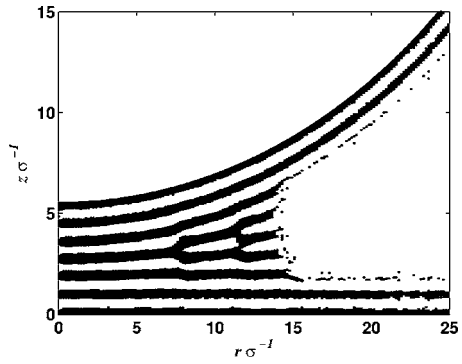

FIG. 4. The shape of liquid meniscus formed between a planar surface and a spherical asperity of the radius $R=36\sigma$ (10 nm), separated at the distance $t=5.5\sigma$. The filled regions on the plot represent areas in which the fluid density exceeds the threshold value of $\rho_{\text{th}}=0.16\sigma^{-3}$. The relative humidity was 90%, and parameters of fluid interaction with solid walls were $\epsilon_s\epsilon^{-1}=1$, and $\alpha\sigma=2$, respectively.

$$-J_{\text{int}}(\rho)=kT \tag{22}$$

or

$$\sigma^3\rho=\frac{3kT}{4\pi\epsilon}\left(\left(\frac{d}{\sigma}\right)^3-1\right)^{-1}. \tag{23}$$

This results in the threshold value between the liquid and vapor phases to be equal to $\sigma^3\rho_{\text{th}}=0.16$. As described in Sec. III A above, the bulk liquid density is $\rho_l=0.731\sigma^{-3}$, while the vapor density is $\rho_v=1.86\times10^{-4}\sigma^{-3}$.

Figure 4 presents the liquid meniscus corresponding to the density profiles plotted in Fig. 3. The spaces of the plot filled with dots correspond to the regions (domain discretization points) in which the fluid density exceeds the threshold value ρ_{th} as defined above.

Figure 5 illustrates the variation of the meniscus's size with respect to the relative humidity H_r. Again, the spaces of the plots filled with dots correspond to the regions in which the fluid density exceeds ρ_{th}. The meniscus boundary shifts to larger values of r as the humidity increases.

Figure 6 shows similar plots for the variable separation t between the walls. The meniscus narrows (as can be seen for $t\sigma^{-1}=2-3$) and eventually disappears ($t\sigma^{-1}=3.5$) as t increases.

C. Fluid-wall interaction parameters: An estimation

The parameters, ϵ_s and α [Eq. (11)] responsible for the energy of the fluid interaction with solid surfaces (ϵ_s), and the spatial range (α) of the corresponding potential, must be estimated for specific surfaces to apply the results of the calculations to real physical systems. The polymolecular ad-

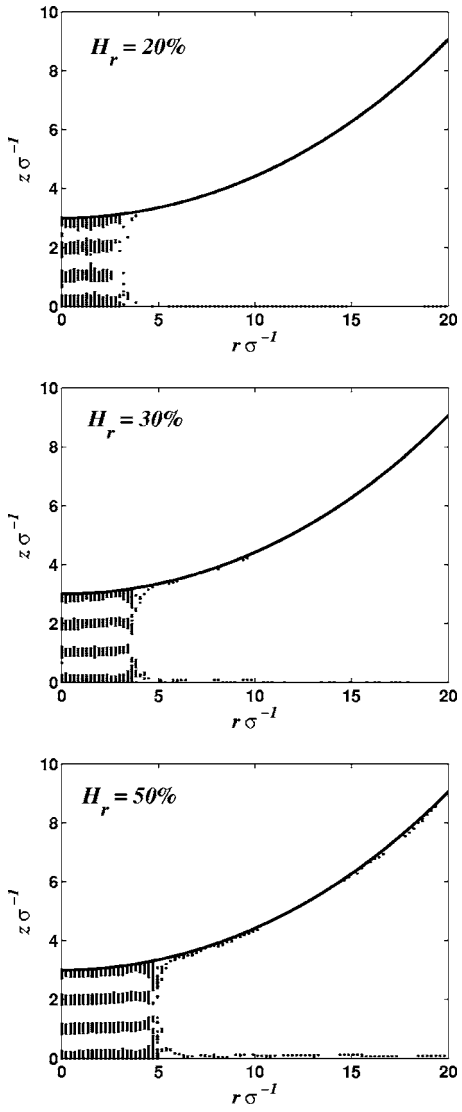

FIG. 5. The variation of the meniscus's size with respect to the relative humidity H_r. The filled regions on the plot represent areas in which the fluid density exceeds the threshold value of $\rho_{th}=0.16\sigma^{-3}$. The parameters are: $t=3\sigma$, $\epsilon_s\epsilon^{-1}=1$, and $\alpha\sigma=2$. The asperity's radius of curvature was $R=36\sigma$.

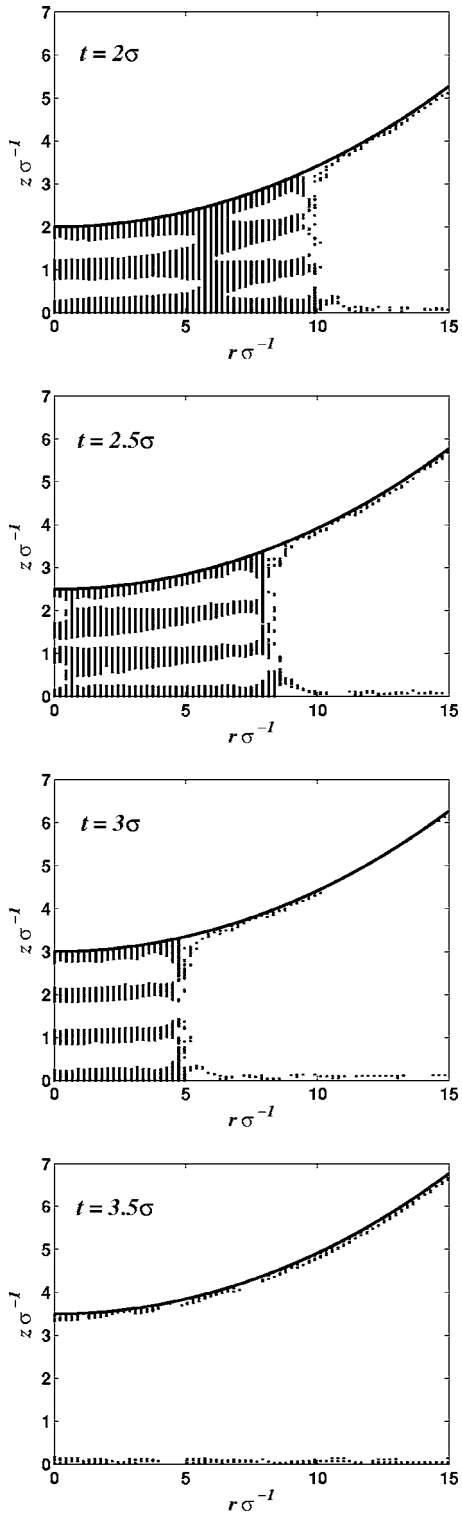

FIG. 6. The variation of the meniscus's size with respect to the separation t between confining surfaces. The filled regions on the plot represent areas in which the fluid density exceeds the threshold value of $\rho_{th}=0.16\sigma^{-3}$. The relative humidity was 50%, parameters of fluid interaction with solid walls were $\epsilon_s\epsilon^{-1}=1$ and $\alpha\sigma=2$. The asperity's radius of curvature was $R=36\sigma$.

sorption isotherms have been used for this purpose because the data of water adsorption is more abundant than those related to the other measurements.

The fluid-wall interaction potential (11) is two-parametric. First, we restrict the potential to act in the region of thickness about σ near the surface by setting $\alpha\sigma=2$. Then the adsorption isotherms for the model fluid on surfaces with different values of ϵ_s are calculated.

The number of molecules adsorbed per surface area of σ^2 (integrated or Gibbs adsorption) with respect to the relative humidity H_r for $T=300$ K is presented in Fig. 7. The Gibbs adsorption was calculated integrating the equilibrium fluid density profiles, calculated from Eq. (10a) reduced to the quasi-one-dimensional (1D) case. A singularity is observed (not shown in the figure) as the humidity (H_r) approaches 100%, consistent with the thermodynamical requirement.[32] The isotherms exhibit typical steplike structure ($\epsilon_s\epsilon^{-1}\sim 1$) for the intermediate humidity values, similar to the results of calculations based on three-dimensional Ono-Kondo lattice model[33] and experimental data for multilayer adsorption of water.[34] The parameter ϵ_s for specific surface of interest may be evaluated by fitting the adsorption isotherm.

The above considerations imply both geometric and energetic uniformities of the surface. The geometric one means

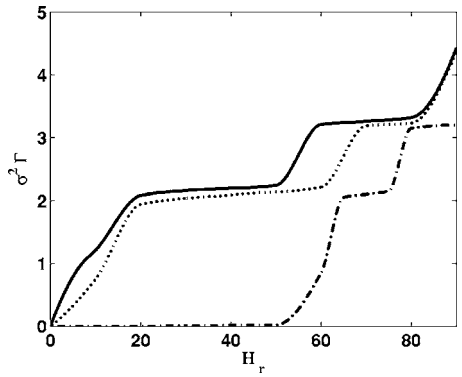

FIG. 7. The adsorption isotherms calculated at different values of $\epsilon_s\epsilon^{-1}$: 1 (dash-dot line), 1.5 (dotted line), 2 (solid line), and with $\alpha\sigma=2$. The function Γ is the number of molecules adsorbed per unit surface area. As H_r approaches 100%, the onset of singularity is observed (not shown).

the average surface roughness is much smaller than the separation distance (t) between surfaces. The latter assumption can be adapted to energetically nonuniform surfaces by taking the effective (average) value of ϵ_s and requiring that the radial region of interest is large enough to sample most of the adsorption energy distribution. Additionally, it is assumed that no significant dissociation of water occurs on the surface, and adsorption is reversible.

IV. SUMMARY

In this study, we have developed a density-functional description for the spatial distribution of the waterlike fluid in proximity of a nanoscale asperity. The approach presents a closed set of procedures modeling the fluid resembling water. The computational part of the approach is adapted for asymmetric geometry of the model comprising two solid surfaces. A bulk behavior of the fluid was used to identify the model parameters and the liquid-vapor coexistence characteristics. The interaction of the fluid with confining walls has been described in the form of the polymolecular adsorption isotherms.

The formation of the liquid meniscus connecting a planar surface and a spherical asperity have been studied in the framework of the developed DFT approach. The influence of the relative humidity and the separation of the confining walls have been investigated. The route for quantitative predictions on the water meniscus formation near atomic force microscope tip dwelling above a sample surface is one of the important applications of the developed methodology. The menisci instabilities related to the tip-substrate distance variations dependent on the AFM lever thermal fluctuations, and also on other factors, could be described in the framework of the current DFT formulation.

This study provides a basic framework for the density-functional description of the case with electric-field-induced anisotropy in the fluid, important for the SPM lithography applications. Additionally, it suggests a way to calculate solvation forces acting on the nanoasperity, based on the surface excess grand free energy available in the density-functional formalism. Such calculation may be used for a molecular level understanding of the AFM force-distance measurements.

ACKNOWLEDGMENT

This work was supported through AFOSR Grant No. F49620-02-1-428 in the frames of Akron/Air Force Center of Polymer Photonics.

[1] B. Capella and G. Dietler, Surf. Sci. Rep. **34**, 1 (1999).
[2] R. Piner and C. Mirkin, Langmuir **13**, 6864 (1997).
[3] H. Bloess, G. Staikov, and J. Schultze, Electrochim. Acta **47**, 335 (2001).
[4] S. Lyuksyutov, P. Paramonov, I. Dolog, and R. Ralich, Nanotechnology **14**, 716 (2003).
[5] R. Piner, J. Zhu, F. Xu, S. Hong, and C. Mirkin, Science **283**, 661 (1999).
[6] S. Hong and C. Mirkin, Science **288**, 1808 (2000).
[7] S. Lyuksyutov, R. Vaia, P. Paramonov, S. Juhl, L. Waterhouse, R. Ralich, G. Sigalov, and E. Sancaktar, Nat. Mater. **2**, 468 (2003).
[8] S. Lyuksyutov, P. Paramonov, R. Sharipov, and G. Sigalov, Phys. Rev. B **70**, 174110 (2004).
[9] S. Lyuksyutov, R. Vaia, P. Paramonov, and S. Juhl, Appl. Phys. Lett. **83**, 4405 (2003).
[10] S. Juhl, D. Phillips, R. Vaia, S. Lyuksyutov, and P. Paramonov, Appl. Phys. Lett. **85**, 3836 (2004).
[11] M. Calleja, M. Tello, and R. Garcia, J. Appl. Phys. **92**, 5539 (2002).
[12] S. Gomez-Monivas, J. Saenz, M. Calleja, and R. Garcia, Phys. Rev. Lett. **91**, 056101 (2003).
[13] S. Rozhok, P. Sun, R. Piner, M. Lieberman, and C. Mirkin, J. Phys. Chem. B **108**, 7814 (2004).
[14] T. Stifter, O. Marti, and B. Bhushan, Phys. Rev. B **62**, 13667 (2000).
[15] C. Gao, Appl. Phys. Lett. **71**, 1801 (1997).
[16] J. Jang, G. Schatz, and M. Ratner, J. Chem. Phys. **116**, 3875 (2002).
[17] J. Jang, G. Schatz, and M. Ratner, Phys. Rev. Lett. **90**, 156104 (2003).
[18] J. Jang, G. Schatz, and M. Ratner, Phys. Rev. Lett. **92**, 085504 (2004).
[19] K. Binder and D. Landau, J. Chem. Phys. **96**, 1444 (1992).
[20] L. Gelb, K. Gubbins, R. Radhakrishnan, and M. Sliwinska-Bartkowiak, Rep. Prog. Phys. **62**, 1573 (1999).
[21] *Applications of the Monte Carlo Method in Statistical Physics*, edited by K. Binder (Springer, New York, 1984).
[22] H. Rafii-Tabar, Phys. Rep. **325**, 239 (2000).
[23] R. Evans, in *Fundamentals of Inhomogeneous Fluids*, edited by D. Henderson (Dekker, New York, 1992), pp. 85–175.
[24] H. Davis, *Statistical Mechanics of Phases, Interfaces and Thin Films* (VCH, New York, 1996), Chap. 12.
[25] N. Carnahan and K. Starling, J. Chem. Phys. **53**, 600 (1970).
[26] T. Vanderlick, L. Scriven, and H. Davis, J. Chem. Phys. **90**, 2422 (1989).
[27] P. Tarazona, Phys. Rev. A **31**, 2672 (1985).
[28] M. Wertheim, J. Stat. Phys. **35**, 19 (1984).
[29] A. Ben-Naim, *Statistical Thermodynamics for Chemists and Biochemists* (Plenum, New York, 1992), Chap. 7.
[30] P. Tarazona, U. M. B. Marconi, and R. Evans, Mol. Phys. **60**, 573 (1987).
[31] H. Stanley, *Introduction to Phase Transitions and Critical Phenomena* (Oxford University Press, London, 1971).
[32] J. Toth, in *Adsorption: Theory, Modeling and Analysis*, edited by J. Toth (Dekker, New York, 2002), pp. 1–103.
[33] G. Aranovich and M. Donohue, J. Colloid Interface Sci. **189**, 101 (1997).
[34] M. Foster and G. Ewing, Surf. Sci. **427–428**, 102 (1999).